Solar Energy Materials & Solar Cells ▮ (▮▮▮▮) ▮▮▮–▮▮▮

Contents lists available at ScienceDirect

Solar Energy Materials & Solar Cells

journal homepage: www.elsevier.com/locate/solmat

Improving light absorption in organic solar cells by plasmonic contribution

David Duche [a], Philippe Torchio [a,*], Ludovic Escoubas [a], Florent Monestier [a], Jean-Jacques Simon [a], François Flory [b], Gérard Mathian [a]

[a] Aix-Marseille University, Institut Matériaux Microélectronique Nanosciences de Provence-IM2NP, CNRS-UMR 6242, Domaine Universitaire de Saint-Jérôme, Service 231, 13397 Marseille Cedex 20, France

[b] Ecole Centrale Marseille, IM2NP CNRS-UMR 6242, Technopôle de Château-Gombert, 38 rue Frédéric Joliot Curie, 13451 Marseille Cedex 20, France

ARTICLE INFO

Article history:
Received 4 December 2008
Received in revised form
20 February 2009
Accepted 25 February 2009

Keywords:
Organic solar cells
Surface plasmon
Absorption enhancement
Bulk heterojunction
FDTD

ABSTRACT

Plasmonic phenomenon inside the materials composing an organic solar cell based on a photoactive poly(2-methoxy-5-(2′-ethyl-hexyloxy)-1,4-phenylenevinylene):(6,6)-phenyl-C_{61}-butyric-acid-methyl ester (MEH-PPV:PCBM) bulk heterojunction is studied using Finite Difference Time Domain (FDTD) method calculations and the modeling results are compared with experimental results.

Enhanced absorptance of light up to 50% is experimentally obtained in a 50-nm-thick blend layer including spin-coated silver nanospheres with a diameter of 40 nm. FDTD calculations based on the design of 2D-grating of nanoparticles confirm the high values of absorptance. Spatial distributions of electromagnetic field power density in the structures show confinement of the power at the interface or in the vicinity of the nanoparticles depending on the wavelength and on the preferential directions.

1. Introduction

In order to produce low-cost energy without green house effect, photovoltaic materials are fabricated in thin film form and strategies are developed to increase light harvesting in the films. New photonic concepts are currently developed by numerous researchers in the photovoltaic domain in order to improve the collection efficiency of light inside cells based on crystalline silicon, thin film silicon, or organic materials: new surface micro- or nanostructuration techniques [1], optimization of the electromagnetic (e.m.) field distribution [2,3], realization of photonic crystals by bulk structuration [4], plasmonic excitation using metallic nanoparticles (NPs) [6–11], etc.

A surface plasmon is an optically generated wave, which propagates along a metal/dielectric interface. In tuning the light excitation, a resonance can occur when the frequency of the incident photons equals the collective oscillation frequency of conduction electrons of metallic particles. In photonics, this domain is known as appellation plasmonics. Among a wide field of applications, these properties can be used in the photovoltaic domain in order to improve the photonic absorption, thus the solar cell efficiency, in particular in the spectral bands where materials absorb weakly. Some noble metal particles such as silver or gold can increase absorption in the visible range. A plasmon can be due to the interaction between a metallic surface (non-localized plasmon) or metallic nanoparticles (localized plasmon) and the light, more precisely between charges (conduction electrons) and electromagnetic waves [5]. The aim of our study is to excite localized plasmons by using metallic NPs to trap or confine light inside the photoactive material, or to obtain beneficial resonant internal light scattering on these metallic particles. This excitation depends on several parameters such as nature of the metal, surface density of the particles, their diameter, incident angle of light, wavelength, polarization, etc. Light absorption could then be amplified, in particular in the spectral ranges where the photovoltaic material absorbs weakly only the light.

A few years before, thin film amorphous silicon solar cells containing 100-nm-diameter gold nanoparticles have been manufactured by Derkacs et al. [6] to engineer the transmission and spatial distribution of the electromagnetic field in visible spectrum inside the a-Si:H layer. Thus, an increase of 8.1% on the short-circuit current density and of 8.3% on the energy conversion efficiency was observed in comparison to the values achieved in reference devices without the gold particles. The authors attributed this improved performance to scattering from surface plasmon polaritons in nearby metallic NPs. Pillai et al. [7] found that surface plasmons can increase the response of crystalline silicon cells over the visible as well as the near-infrared spectra. They reported a significant enhancement of the absorptance for both 1.25-μm-thick film and wafer-based 300-μm-thick crystalline planar silicon structures including silver

* Corresponding author.
E-mail address: philippe.torchio@univ-cezanne.fr (P. Torchio).

0927-0248/$ - see front matter © 2009 Elsevier B.V. All rights reserved.
doi:10.1016/j.solmat.2009.02.028

islands of 12 and 16 nm diameters. The photocurrent response was increased by about 30% over the whole visible range, and also in the near-infrared with a factor of 16 at $\lambda = 1050$ nm. This light trapping approach, also based on scattering by particles in silicon devices, clearly allows amplifying the interaction between light and material. Schaadt et al. [8] reported an engineered enhancement of optical absorptance and photocurrent in silicon p–n junction via the excitation of surface plasmon resonances in spherical Au nanoparticles and suggested their use for improving performances of photodetectors, imaging arrays and photovoltaics. Similar studies were carried out with organic materials to enhance light absorptance, subsequently leading to an increase in the amount of excitons. Stenzel et al. [9] have already demonstrated in systems ITO/NPs/CuPc/In that incorporating copper or gold NPs was increasing the photocurrent by a factor of more than two. This result was then confirmed by Westphalen et al. [10] on components such as ITO/Ag clusters/ZnPc/Ag in which the exciton rate was increased resulting in a photocurrent multiplied by a factor of two. Rand et al. [11] have studied the optical properties of NPs and have shown that enhancing electromagnetic field by plasmonic excitation allows to increase conversion efficiency of tandem organic cells by increasing the excitation generation rate. Their multilayer device ITO/CuPc/PTCBI/silver NPs/CuPc/PTCBI/Ag consisted of a serial connection of two donor–acceptor heterojunctions separated by a very thin layer of metallic nanoagregates, which were used as charge recombination centers. They also exhibited an increased absorptance by a factor of 2, for 7-nm-thick CuPc single layers including 1-nm-diameter silver NPs in comparison with single layers without these NPs.

The work presented in this paper aims at studying the potentiality of this plasmonic technique on cells, of which the active layer is composed by an interpenetrated donor–acceptor blend and it also aims at modeling this phenomenon by using a software based on the Finite Difference Time Domain (FDTD) method [12]. A bulk heterojunction (BHJ) device has been chosen because this kind of photoactive material is very promising and, presently, exhibits the best photovoltaic efficiencies in the field of organic solar cells [13].

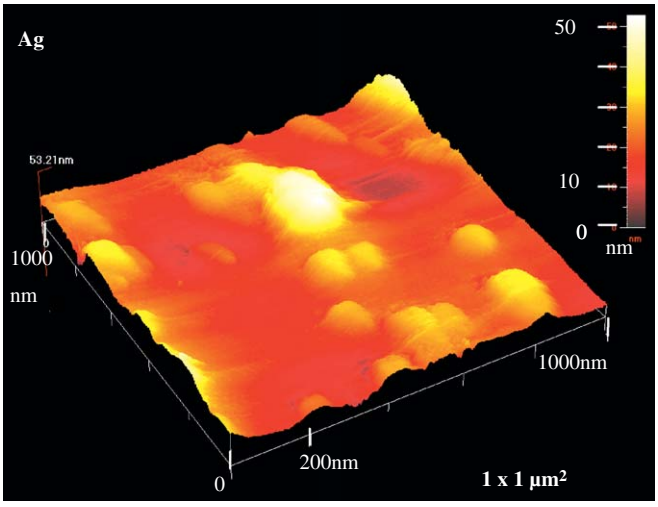

Fig. 1. Atomic force microscopy (AFM) image of silver nanoparticles spin-coated on a SiO_2 substrate.

2. Results and discussion

2.1. Experimental

Photoactive layers were fabricated from an interpenetrated network of conjugated polymer poly(2-methoxy-5-(2′-ethyl-hexyloxy)-1,4-phenylenevinylene) (MEH-PPV) as electron donor and fullerene derivative (6,6)-phenyl-C_{61}-butyric-acid-methyl ester (PCBM) as electron acceptor. These layers were deposited on silica substrates, after incorporation of silver nanoparticles in some of the samples.

SiO_2 substrates were first sequentially cleaned in an ultrasonic bath by using acetone and isopropanol, then rinsed with deionised water, dried in an oven at 120 °C for 30 min and finally treated with UV-generated ozone. Colloïdal solutions rich in spherical silver nanoparticles with diameter 40 nm were spin-coated on the silica substrates. These NPs were diluted in 10%wt. ethylene glycol. The adhesion of NPs on the silica surface was previously ensured by dip-coating the substrates in an organosilane (APTMS: 3-aminopropyl trimethoxysilane) in ethanol solution. This latter step also allows avoiding a too strong aggregation of the nanoparticles and preventing particle migration in the film. The parameters of these inhomogeneous metallic deposits have been adjusted to obtain coalescent deposits as thin as possible, with a control by atomic force microscopy (AFM) as shown in Fig. 1. We observe a random array of silver clusters of about 100 nm width and 40 nm height. If the lateral size is higher than that of one isolated particle, the height is well conserved. Some substrates, with or without NPs, were then covered by spin-coating a bulk heterojunction from an anhydrous chlorobenzene solution of MEH-PPV:PCBM at 1:4 weight ratio (Fig. 2). The films were spun at 1500 rpm during 1 min. The thickness of the film was 50 nm, measured by using a mechanical profilometer.

Spectrophotometric measurements of the reflectance (R) and the transmittance (T) allows to deduce the values of absorptance (A) and scattering (S) $A+S = 1-R-T$ of these samples in the visible range (Fig. 3). We clearly observe an improvement of $(1-R-T)$ over a broad spectral range between 375 and 800 nm for stacks including NPs, with a maximum gain of 50% at 500 nm compared to those without NPs. In the 375–575 nm spectral domain, the improvement of $(A+S)$ in the polymer:fullerene heterojunction including NPs can be mainly attributed to a plasmonic effect inside the heterojunction while, in the 575–800 nm region, the improved $(A+S)$ values could be essentially due to the absorptance and scattering of the NPs themselves.

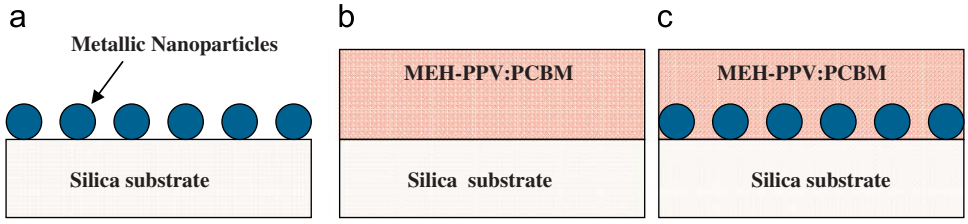

Fig. 2. Structure of the fabricated samples: (a) silica/silver nanoparticles, (b) silica/MEH-PPV:PCBM 1:4 and (c) silica/silver nanoparticles/MEH-PPV:PCBM 1:4.

Please cite this article as: D. Duche, et al., Sol. Energy Mater. Sol. Cells (2009), doi:10.1016/j.solmat.2009.02.028

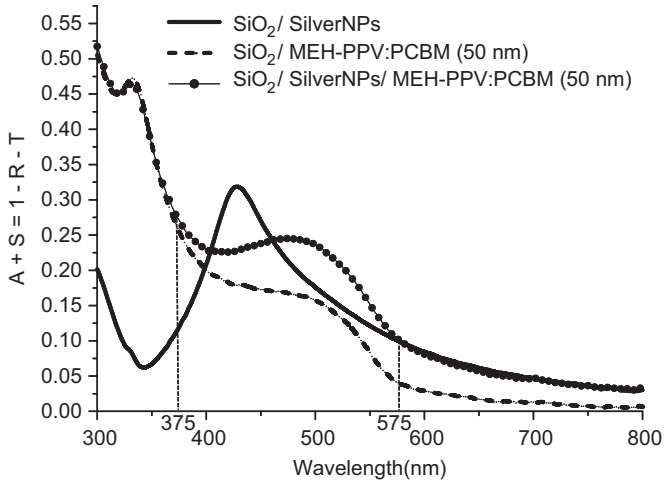

Fig. 3. Values of $A+S=1-R-T$ deduced from spectrophotometric measurement of reflectance and transmittance for the devices: silica/silver nanoparticles (solid line), silica/MEH-PPV:PCBM 1:4 without (dotted line) or with silver nanoparticles (filled circles line).

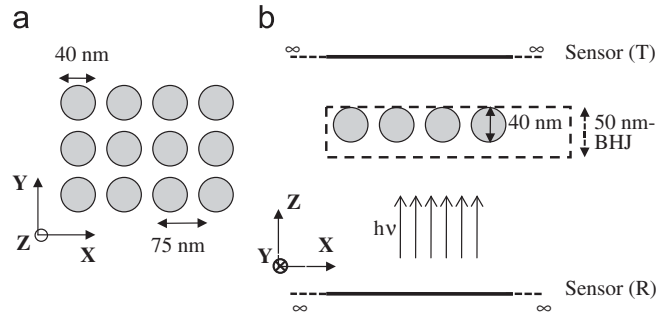

Fig. 4. Schematics of the metallic nanospheres in a 2D-grating design, embedded or not in a bulk heterojunction film, used for FDTD calculations: (a) top view and (b) side view.

2.2. Numerical model

In order to understand the *A+S* mechanisms previously shown in Section 2.1, the absorptance was calculated and the electromagnetic field was modeled, thanks to a Finite Difference Time Domain method. The numerical FDTD method [12] allows solving the Maxwell's equations versus time on a discrete spatial grid. Moreover, a discretization of time Δt allows taking into account the propagation phenomenon of the electromagnetic field. To perform the calculation of light propagation through a structure, several numerical parameters have to be considered, e.g., finite computational domain (x, y, z), the boundary conditions as the periodicity properties of the structures, spatial grid sizes (Δx, Δy, Δz), temporal grid Δt and thus, the computation time, relative permittivity $\varepsilon(\mathbf{r}, \omega)$ and relative permeability $\mu(\mathbf{r}, \omega)$ for each material of the structure, etc.

We modeled previous structures but with a simplified design constituted of a two-dimensional (2D) array of silver nanospheres having a 40 nm diameter rather than an inhomogeneous and coalescent layer. As shown in Fig. 4, the structure had 2D-grating composed of a squared lattice with a period equal to 75 nm. This structure was first placed in the air as the surrounding medium, then embedded in a host matrix of 50-nm-thick MEH-PPV:PCBM blend. It is important to notice that, for the calculation, each device was illuminated with plane waves in normal incidence, while reflectance (R) and transmittance (T) were calculated using two infinite sensors, which received all the reflected and transmitted energies (Fig. 4b), including in particular the non-specular reflected part. If it exists, the scattered light would be included here in the non-specular reflectance. It means that the absorptance in the device is then obtained by $1-R-T$. Sensors were considered sufficiently far from the device to avoid near-field effects. The temporal grid was $\Delta t = 17\times10^{-19}$ s and the spatial grid was $\Delta x = \Delta y = \Delta z = 0.9$ nm. Computations have been performed using monochromatic excitations at wavelengths ranging between 350 and 800 nm. The polarization state TE or TM of the light has no influence because computations were done in normal incidence. Nevertheless, in order to have a better understanding of the phenomena, we decided to keep only the E_x component along the x-axis of the electrical field of the incident light and to cancel the E_y component along the y-axis.

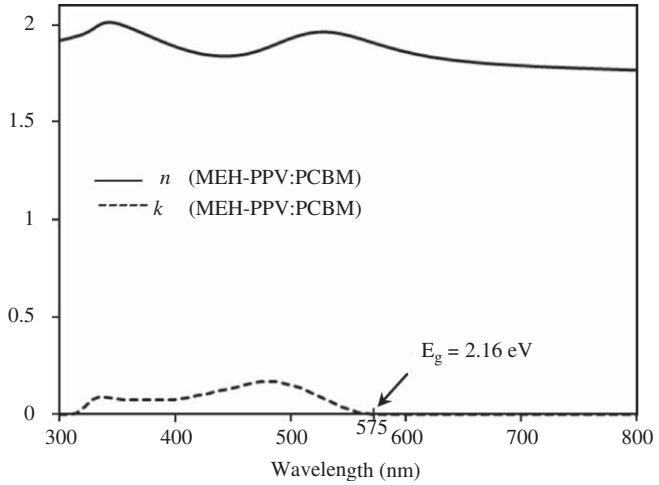

Fig. 5. Dispersion curves obtained by spectroscopic ellipsometry representing the real (full line) and the imaginary (dotted line) parts of the complex refractive index of the MEH-PPV:PCBM bulk heterojunction.

Furthermore, the dispersion curves of the complex refractive indices of the materials have to be taken into account. Real and imaginary parts of the complex refractive index, n and k, of MEH-PPV:PCBM, deduced from experimental ellipsometric measurements performed by SOPRA S.A. company (Fig. 5), have been introduced in the computation for each wavelength. The energy gap of the considered bulk heterojunction is found to be equal to 2.16 eV ($\lambda = 575$ nm). Refractive index dispersion curves of silver in thin film form were obtained by fitting the experimental ellipsometric data found in the literature [14]. A fit of metallic material parameters by using only a Drude or Drude–Lorentz model is highly recommended in our FDTD software. The Drude model given by Eq. (1) was then used as a fit law for the complex dielectric constant of silver:

$$\varepsilon_m(\omega) = \varepsilon_{inf} + \Delta/(-a\omega^2 - ib\omega) = (n + ik)^2 \quad (1)$$

The obtained constants were $\varepsilon_{inf} = 5$, $\Delta = 2181.58$, $a = 1.11\times10^{-17}$ and $b = 5.79\times10^{-9}$.

Comparison between fitted data and measured data for optical constants n and k of silver are shown in Fig. 6. The differences are due to the fact that law (1) has to be validated by the two parts of the complex dielectric constants, i.e. both n and k.

2.3. Numerical results

We have computed by the FDTD method the reflectance (R), the transmittance (T) and the deduced absorptance (A) from the equation $1-R-T$. R, T and A are presented in Fig. 7 versus wavelength for the metallic 2D-structure depicted in Fig. 4 and placed in the air. A surface plasmon effect at the surface of the

Please cite this article as: D. Duche, et al., Sol. Energy Mater. Sol. Cells (2009), doi:10.1016/j.solmat.2009.02.028

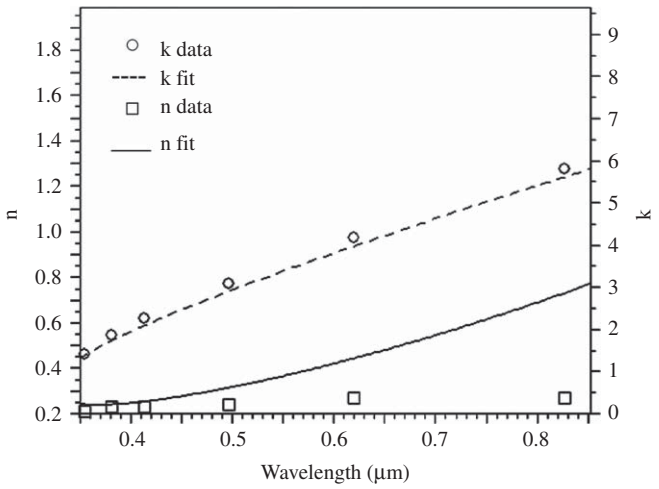

Fig. 6. Measured data from [12] compared with our fitted data with a Drude model (used as input in our numerical method) for optical constants of silver.

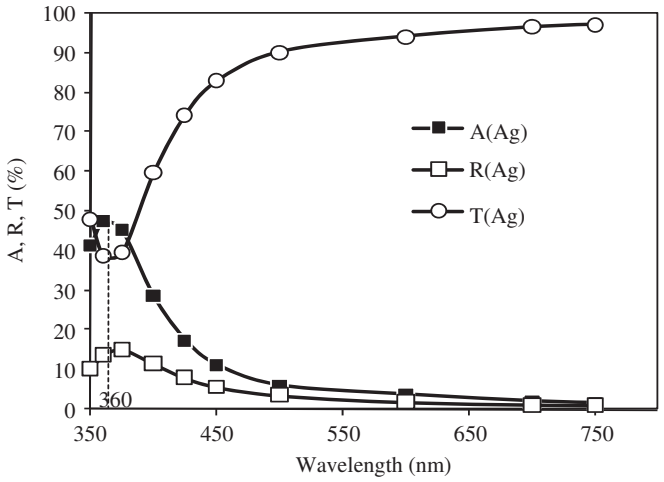

Fig. 7. Calculated values of reflectance (□), transmittance (○) and absorptance ($1-R-T$) (■) versus wavelength for a square matrix of silver nanoparticles placed in air. Plasmon resonance at $\lambda = 360$ nm.

nanospheres appears, which results in a strong decrease of the transmission and then an increase of the absorptance, at wavelength 360 nm. Nevertheless, a maximum appears also on the R curve at $\lambda = 375$ nm. We can also attribute this small peak to the surface plasmon, which could cause a decoupling of light in the plane of periodicity of the NPs grating and an increase of R, as it was noticed in [15] in similar coupling devices using photonic crystals. Because our 2D structure exhibits a dual periodicity of the dielectric constant, it can be considered as a 2D photonic crystal, but this appellation is usually used for all dielectric structures.

The diameter of the nanospheres is very small compared to the wavelengths of the incident waves. Thus, the Mie Theory [16] can be used to describe the interaction of the incident energy with the localized plasmons due to the metallic nanoparticles. This model consists of the rigorous resolution of Maxwell's equation by taking both the electromagnetic field inside the NPs and the field scattered by the NPs into account. The first-order Mie Theory leads to the expression of the extinction coefficient $\sigma(\omega)$, also called "absorption-scattering cross-section", of a set of metallic NPs [17]

$$\sigma(\omega) = \frac{9N\omega V\varepsilon_s^{3/2}}{c}\left(\frac{\varepsilon_2(\omega)}{[\varepsilon_1(\omega)+2\varepsilon_s(\omega)]^2+\varepsilon_2^2(\omega)}\right) \quad (2)$$

where $\omega = 2\pi/\lambda$ is the pulsation of the incident electromagnetic field, c the speed of light in vacuum, ε_s the dielectric constant of the surrounding medium, V the volume of one NP, N the volumic density of NPs, and ε_1 and ε_2 are, respectively, the real part and the imaginary part of the dielectric constant ε_m of the metal ($\varepsilon_m = \varepsilon_1 + i\varepsilon_2$). It is important to notice that both scattering out of the NPs and absorption inside the NPs are included in $\sigma(\omega)$.

According to Eq. (2), $\sigma(\omega)$ is maximal when $[(\varepsilon_1(\omega)+2\varepsilon_s(\omega))^2+\varepsilon_2^2(\omega)]$ is equal to zero. This condition is called the Mie resonance.

Thus, assuming that $\varepsilon_1^2 \gg \varepsilon_2^2$ for frequencies in the Mie resonance region (typically true for Ag), Mie Theory can predict the plasmon resonance wavelength of a layer integrating NPs by using the following formula:

$$\varepsilon_1(\omega) = -2\varepsilon_s(\omega) \quad (3)$$

According to Eq. (3) and silver optical constants, we calculate and obtain the plasmon resonance wavelength at $\lambda = 357$ nm. A very close value of that resonance wavelength is observed in Fig. 7 ($\lambda = 360$ nm).

In order to highlight and explain the experimental plasmon effect by numerical calculation, we have calculated values of ($1-R-T$), i.e. absorptance, versus the wavelength for a squared 2D-grating silver nanoparticles placed in the air, for the MEH-PPV:PCBM interpenetrating network alone, and for silver nanoparticles embedded in the network (Fig. 8). Even if the Ag distribution is slightly different in our experiments and in our calculations, we observe that the main behaviour of the three calculated curves is similar to experiments curves (see Fig. 3). The behaviour of the absorptance curve concerning the MEH-PPV:PCBM alone is in accordance with those of its extinction coefficient k (Fig. 5), like the value of the energy gap at 575 nm. The enhancement of the absorptance for samples consisting in a blend including NPs in comparison with those without NPs is also clearly observed on a large spectral range ($350\,\text{nm} < \lambda < 800\,\text{nm}$). This enhancement is attributed to the localized plasmon effect due to the metallic NPs. We can also notice that the plasmon resonance wavelength is redshifted by 95 nm to $\lambda = 455$ nm in comparison with the resonance at $\lambda = 360$ nm of the NPs placed in air. This result fulfils the Mie Theory of Eq. (2), which shows that the plasmon resonance depends on the "difference" between the real part of the relative permittivity of the metal and the relative permittivity of the host material surrounding the nanospheres (either air or active blend). The beneficial effect is mainly interesting in the long-wavelength range $500\,\text{nm} < \lambda < 800\,\text{nm}$, in a spectral region where the MEH-PPV:PCBM absorbs weakly or

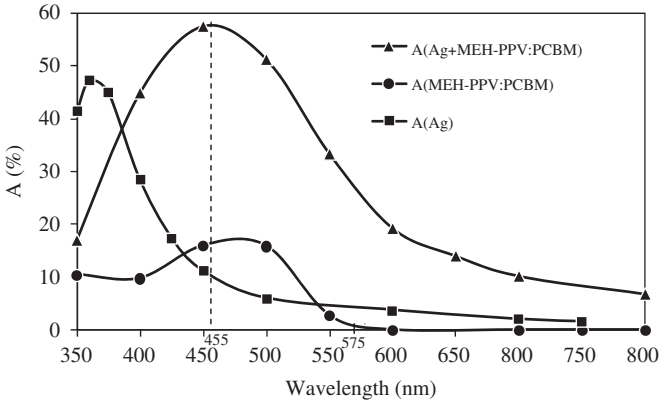

Fig. 8. Calculated values of absorptance $A = (1-R-T)$ versus wavelength for devices: silver nanoparticles in air (■), MEH-PPV:PCBM alone (●), and silver nanoparticles embedded in MEH-PPV:PCBM (▲) showing a resonance at $\lambda = 455$ nm.

Please cite this article as: D. Duche, et al., Sol. Energy Mater. Sol. Cells (2009), doi:10.1016/j.solmat.2009.02.028

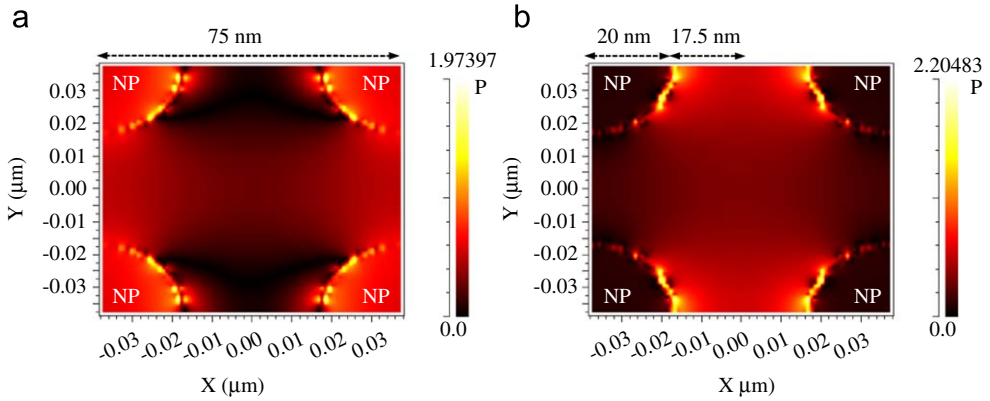

Fig. 9. Spatial distribution of the power density P of the electromagnetic field in the nanoparticles plane $\{x, y\}$ and in the dielectric vicinity of an array of 4 silver NPs at the incident wavelength of: (a) 450 nm and (b) 600 nm.

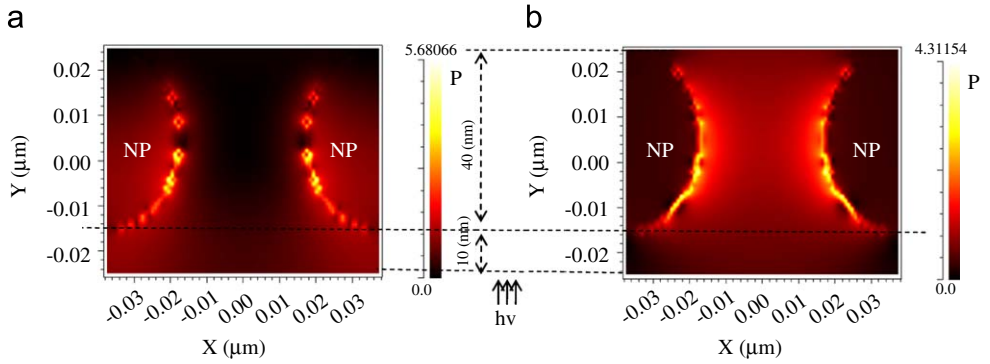

Fig. 10. Spatial distribution of the power density P of the electromagnetic field in the orthogonal plane $\{x, z\}$ of the NPs and in the dielectric vicinity of an array of 2 silver NPs at the incident wavelength of: (a) 450 nm and (b) 600 nm.

very weakly, while the metal has a very low level of absorptance. In this spectral region, the absorptance gain in the solar cell can be very strong. In the other part of the spectrum, $350\,\text{nm} < \lambda < 500$ nm, the absorptance in the metal is not negligible, as shown on the curve of the NPs in air, and the absorptance of the plasmon structures may not be profitable to the final device performance. However, the solar spectral intensity at $\lambda < 350$–400 nm is rather weak and does not critically impact the performances as compared with longer wavelengths.

Therefore, it would be interesting to separate the contribution of the absorptance due to the metallic nanospheres from that of the bulk heterojunction. Our numerical FDTD method is able to calculate and to map the distribution of the power density (P) carried by the electromagnetic plane wave in our plasmonic structure. This value of P power flow is calculated over one period in steady state and can be thought of as a type of time average. P can also represent the modulus of the Poynting vector. Fig. 9(a) shows the spatial distribution of the power density of the e.m. field in the nanoparticles plane $\{x, y\}$ and in the dielectric vicinity of an array of 4 silver NPs at the excitation wavelength 450 nm in normal incidence (direction z). This wavelength is very close to the maximum absorptance peak of the NPs embedded in the BHJ (455 nm). We locally observe a very strong increase of the power density at the interface between the blend and the NPs ("bright areas"), a non-negligeable level inside the NPs, and also a mean level of P in the blend surrounding the NPs, which occurs preferentially along the x-axis in the plane of the squared lattice (which is in accordance with the E_x incident electrical field orientation). At the interface between both media, in the internal side of NP, the distance where P decreases exponentially down to P/e is in agreement with the value of silver skin thickness (between 2.5 and 3 nm for wavelengths ranging between 450 and 600 nm). Results confirm that silver is able to absorb a part of the incident light at $\lambda = 450$ nm. At the excitation wavelength of 600 nm, corresponding to a low-level absorptance of BHJ with NPs, the power density is decreased inside the NPs and beneficially enhanced in the interface and in the dielectric medium between NPs along the x-axis (Fig. 9(b)). The maximal P-values are enhanced from 1.97 at $\lambda = 450$ nm to 2.2 at $\lambda = 600$ nm. The P-values are referred to the incident power density value which equals 1. Along this x-axis, we can notice in the Fig. 9(b) that the power enhancement is produced significantly in the interstice up to the midpoint between 2 NPs, i.e. 17.5 nm. Other P distributions carried out across the z-axis transversal to the 2D-array are presented in Figs. 10(a) and (b). Fig. 10(a), computed at $\lambda = 450$ nm, confirms the very strong increase of P at the interface between the NPs and the environment (with values up to 5.68). At $\lambda = 600$ nm, the P enhancement is mainly confined in the medium between the NPs (Fig. 10(b)), thus improving the absorptance of light in the BHJ film. In figures (a) and (b), we observe that the increase in P is prolonged in the whole embedded medium along the z-axis up to about 10 nm out of the NP (corresponding to the limit of the BHJ thickness in our design) towards the light source. Power density enhancements happening along preferential directions, are very promising for multilayer organic solar cells applications. Indeed, it is observed in our computations that the interaction length between light and matter can be significantly increased.

3. Conclusion

We investigate the absorption enhancement induced by silver nanoparticles within a dielectric layer. Experimental results were

Please cite this article as: D. Duche, et al., Sol. Energy Mater. Sol. Cells (2009), doi:10.1016/j.solmat.2009.02.028

obtained by using a spin-coating method to spread the colloidal nanoparticles on wide areas of organosilane-coated silica substrates. Enhanced absorptance up to 50% was obtained for a bulk heterojunction layer including these nanospheres. Power density of the electromagnetic field computations confirms that an increased absorptance and increased concentration of the power are possible in the vicinity of a two-dimensional array of nanoparticles embedded in the BHJ. Preferential distributions of the electromagnetic field in the longitudinal and transversal planes with respect to the nanoparticles 2D-grating are shown. Both effects, the increase of the local field strength and the internal light scattering, can contribute to stronger absorption. The investigation has to be completed by optical measurements in order to separate the contribution to the global absorption from possible external scattering. The best positioning of these nanoparticles in a multilayer organic solar cell has to be analyzed in order to maintain the strong benefit of the localized surface plasmons on absorption without degrading the electrical properties, and thus to obtain a significant photovoltaic power efficiency improvement.

Acknowledgements

The authors acknowledge C. Defranoux from SOPRA S.A. company (Bois Colombes-France) for spectroscopic ellipsometry measurements of MEH-PPV:PCBM, and Agence Nationale de la Recherche (ANR) for support under the photovoltaic program SPARCS (ANR-07-PSPV-006-02).

References

[1] F. Flory, L. Escoubas, B. Lazarides, Artificial anisotropy and polarizing films, Appl. Opt. 41 (16) (2002) 3332–3335.
[2] F. Monestier, Ph. Torchio, J.J. Simon, L. Escoubas, M. Cathelinaud, Demonstration of a software for automatic optimization of the electromagnetic field in organic solar cells, Nonlinear Opt. Quantum Opt. 37 (2007) 159–168.
[3] F. Monestier, J.J. Simon, Ph. Torchio, L. Escoubas, F. Flory, S. Bailly, R. de Bettignies, S. Guillerez, C. Defranoux, Modeling the short circuit current density of polymer solar cells based on P3HT:PCBM blend, Sol. Energ. Mater. Sol. Cells 91 (2007) 405–410.
[4] D. Duche, L. Escoubas, J.J. Simon, Ph. Torchio, W. Vervisch, F. Flory, Slow bloch-modes for enhancing the absorption of light in thin films for photovoltaic cells, Appl. Phys. Lett. 92 (2008) 193310.1–193310.3.
[5] W.L. Barnes, A. Dereux, T.W. Ebbesen, Surface plasmon subwavelength optics, Nature (London) 424 (2003) 824–830.
[6] D. Derkacs, S.H. Lim, P. Matheu, W. Mar, E.T. Yu, Improved performance of amorphous silicon solar cells via scattering from surface plasmon polaritons in nearby metallic nanoparticles, Appl. Phys. Lett. 89 (2006) 093103.1–093103.3.
[7] S. Pillai, K.R. Catchpole, T. Trupke, M.A. Green, Surface plasmon enhanced silicon solar cells, J. Appl. Phys. 101 (2007) 093105.1–093105.8.
[8] D.M. Schaadt, B. Feng, E.T. Yu, Enhanced semiconductor optical absorption via surface plasmon excitation in metal nanoparticles, Appl. Phys. Lett. 86 (2005) 063106.1–063106.3.
[9] O. Stenzel, A. Stendhal, K. Voigtsberger, C. von Borczyskowski, Enhancement of the photovoltaïc conversion efficiency of copper phthalocyanine thin film devices by incorporation of metal clusters, Sol. Energy Mater. Sol. Cells 37 (1995) 337–348.
[10] W. Westphalen, U. Kreibig, J. Rostalski, H. Lüth, D. Meissner, Metal cluster enhanced organic solar cells, Sol. Energy Mater. Sol. Cells 61 (2000) 97–105.
[11] B.P. Rand, P. Peumans, S.R. Forrest, Long-range absorption enhancement in organic tandem thin-film solar cells containing silver nanoclusters, J. Appl. Phys. 96 (12) (2004) 7519–7526.
[12] A. Tavlove, Computational Electrodynamics: The Finite-Difference Time-Domain Method, Artech House, Norwood, MA, 1995.
[13] J.Y. Kim, K. Lee, N.E. Coates, D. Moses, T. Nguyen, M. Dante, J. Heeger, Efficient Tandem polymer solar cells fabricated by all-solution processing, Science 317 (2007) 222–225.
[14] E.D. Palik, Handbook of Optical Constants of Solids, Academic Press, New York, 1985, p. 12.
[15] C. Seassal, Y. Park, A. Fave, E. Drouard, E. Fourmond, A. Kaminski, M. Lemiti, X. Letartre, P. Viktorovitch, Photonic crystal assisted ultra-thin silicon photovoltaic solar cell, in: SPIE Proceedings of the Photonics Europe Conference, 2008.
[16] G. Mie, Beiträge zur optik trüber medien, Speziell Kolloidaler Metallösungen, Leipzig, Ann. Phys. 330 (1908) 377–445.
[17] U. Kreibig, M. Vollmer, Optical Properties of Metal Clusters, Springer, Berlin, 1995.

Please cite this article as: D. Duche, et al., Sol. Energy Mater. Sol. Cells (2009), doi:10.1016/j.solmat.2009.02.028